Journal of Medicinal Chemistry

Article

pubs.acs.org/jmc

Multimodal Chelation Platform for Near-Infrared Fluorescence/Nuclear Imaging

Sukhen C. Ghosh, Pradip Ghosh, Nathaniel Wilganowski, Holly Robinson, Mary A. Hall, Gabriel Dickinson, Ken L. Pinkston, Barrett R. Harvey, Eva M. Sevick-Muraca, and Ali Azhdarinia*

Center for Molecular Imaging, The Brown Foundation Institute of Molecular Medicine, The University of Texas Health Science Center at Houston, Houston, Texas 77030, United States

ABSTRACT: Dual-labeled compounds containing nuclear and near-infrared fluorescence contrast have the potential to molecularly guide surgical resection of cancer by extending whole-body diagnostic imaging findings into the surgical suite. To simplify the dual labeling process for antibody-based agents, we designed a multimodality chelation (MMC) scaffold which combined a radiometal chelating agent and fluorescent dye into a single moiety. Three dye-derivatized MMC compounds were synthesized and radiolabeled. The IRDye 800CW conjugate, **4**, had favorable optical properties and showed rapid clearance in vivo. Using **4**, an epithelial cell adhesion molecule (EpCAM) targeting MMC-immunoconjugate was prepared and dual-labeled with ^{64}Cu. In vitro binding activity was confirmed after MMC conjugation. Multimodal imaging studies showed higher tumor accumulation of ^{64}Cu-**7** compared to nontargeted ^{64}Cu-**4** in a prostate cancer model. Further evaluation in different EpCAM-expressing cell lines is warranted as well as application of the MMC dual labeling approach with other monoclonal antibodies.

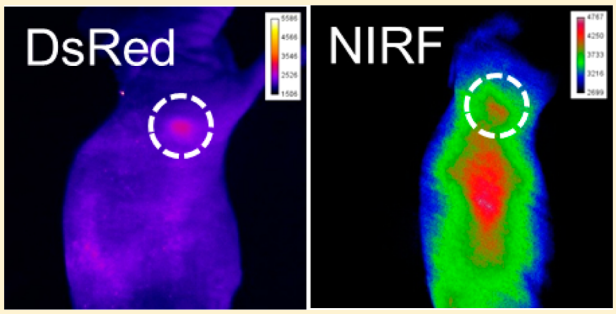

INTRODUCTION

Over the past decade, hybrid imaging technologies have played an important role in the clinical management of cancer patients. The complementary features of functional (i.e., positron emission tomography (PET) or single-photon emission computed tomography (SPECT)) and anatomical (i.e., computed tomography (CT) or magnetic resonance imaging (MRI)) imaging have been combined to improve detection, staging, treatment planning, and therapeutic monitoring in several cancers.[1]

Near-infrared fluorescence (NIRF) imaging, once considered a preclinical tool, promises sensitivity comparable to that of nuclear imaging (femtomolar to picomolar range)[2] and has experienced tremendous translational growth in recent years owing to improvements in device sensitivity and the introduction of new fluorescent contrast reagents for probe development.[3,4] The absence of radioactivity, lack of physical decay, and mobility of imaging devices make optical imaging especially amenable for molecular imaging during surgery. Recently, fluorescence imaging (λ_{em} = 521 nm) has been successfully used for intraoperative imaging in humans with a fluorescently labeled folate analogue,[5] and NIRF (λ_{em} = 830 nm) has been used for noninvasive imaging of lymphatics in humans at microdose levels that are comparable to those of radiotracers.[6] However, in contrast to nuclear imaging techniques, fluorescence imaging requires collection of low-energy photons that can be attenuated and obscure detection for noninvasive, nonsurgical imaging applications. By combining both types of contrast to produce a dual-labeled imaging agent, whole-body nuclear imaging and intraoperative NIRF signals can be obtained from a single administration and enhance the clinical utility of molecular imaging. In addition, the presence of the radioactive signal overcomes the current lack of standardized methods for quantification of imaging and biodistribution data in NIRF imaging. Conceivably, dual-labeled agents could be administered to a patient for whole-body diagnostic nuclear scans and surgical planning, and after isotope decay, the NIRF signal can be used by surgeons to detect diseased tissues and identify tumor margins and residual disease. In contrast to a cocktail approach where separate radioactive and NIRF-labeled agents often have distinct pharmacokinetic (PK) properties and imaging time windows,[7] dual labeling affords an integrated multimodal agent which can be characterized noninvasively by nuclear imaging, intraoperatively by NIRF, and histologically on the basis of the fluorescent signal to confirm molecular targeting.

In this study, we report the synthesis and pharmacological characterization of a multimodal chelation (MMC) scaffold which combined a bifunctional chelating agent (BFCA) and NIRF dye into a single moiety for facile preparation of dual-labeled compounds. The MMC structure was based upon the widely used BFCA 1,4,7,10-tetraazacyclododecane-*N*,*N*′,*N*″,*N*‴-tetraacetic acid (DOTA) to provide versatility for incorporating different radionuclides. Following the synthesis of different MMC−dye conjugates, radiolabeling was

Received: June 27, 2012
Published: December 6, 2012

   dx.doi.org/10.1021/jm300906g | *J. Med. Chem.* 2013, 56, 406−416

Scheme 1. Synthesis of an Amine Derivative of 1[a]

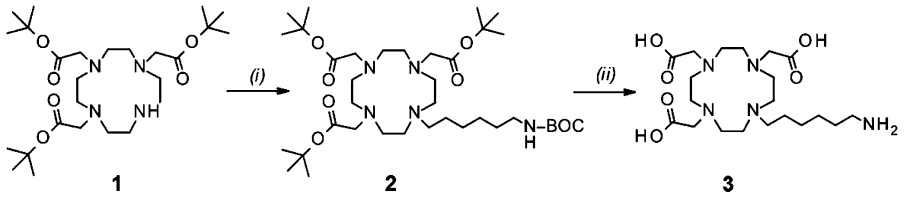

[a]Reagents and conditions: (i) 6-((*tert*-butoxycarbonyl)amino)hexyl bromide, K_2CO_3, CH_3CN, 75 °C, 12 h; (ii) concd HCl (34−37%), 4 h.

Scheme 2. Synthesis of Fluorescently Labeled Derivatives 4−6[a]

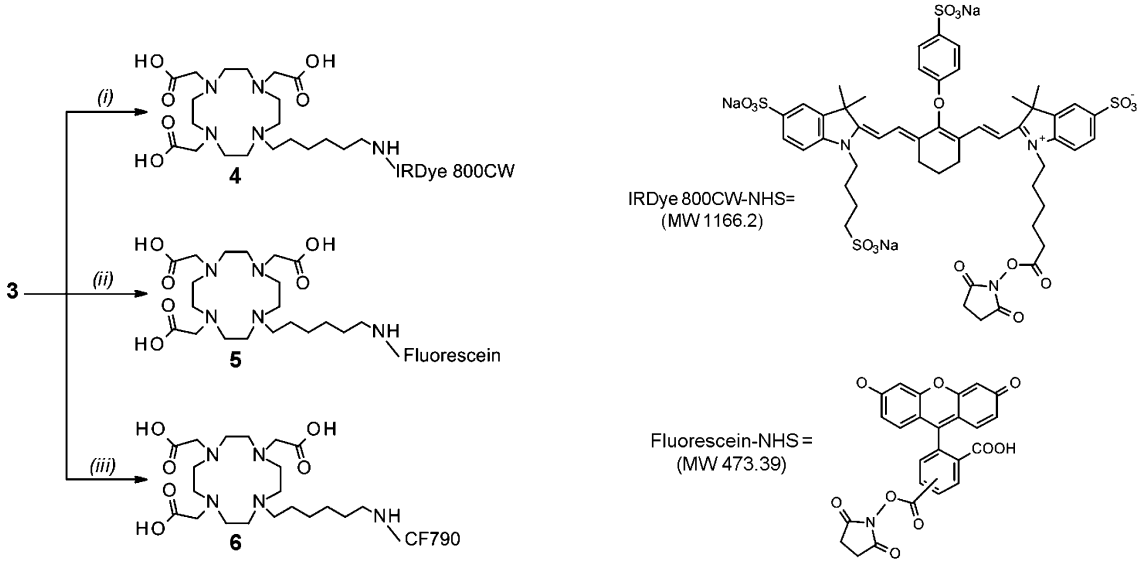

[a]Reagents and conditions: (i) IRDye 800CW−NHS ester; (ii) fluorescein−NHS ester; (iii) CF790−NHS ester; all performed in $NaHCO_3$ buffer (0.1 M, pH 8.5), 4 °C, overnight stirring in the dark.

performed with the positron-emitting radionuclides ^{68}Ga ($t_{1/2}$ = 68 min) and ^{64}Cu ($t_{1/2}$ = 12.7 h), and the optical properties were examined. Multimodal imaging and biodistribution studies were performed to assess the in vivo stability and PK of the dual-labeled analogue of **4** in tumor-free mice. To demonstrate utility of an MMC agent for tumor targeting, we coupled **4** to an epithelial cell adhesion molecule (EpCAM) targeting monoclonal antibody (mAb), dual-labeled with ^{64}Cu, and evaluated the in vitro binding properties in EpCAM-expressing cell lines along with in vivo imaging in mice with prostate cancer.

RESULTS AND DISCUSSION

Among dual-labeled NIRF/nuclear imaging agents in the literature, there are far more reports on peptide-targeted compared to mAb-targeted approaches.[8,9] This may be due to factors such as the narrow window within which mAb chemistry can be conducted without denaturing the molecule and decreasing biological activity, as well as the inability to perform site-specific conjugation to mAbs. A typical preparation of a dual-labeled mAb involves sequential coupling of *N*-hydroxysuccinimide (NHS) ester, maleimide, or isothiocyanate derivatives of a chelating agent and an NIRF fluorophore, followed by radiolabeling.[10−12] In the case of commonly used NHS reagents, the random distribution of lysine residues may cause conjugations to occur in the binding region of the mAb and impair the immunoreactivity of the agent. Therefore, reaction conditions such as pH, buffer, and incubation time require optimization to minimize excessive conjugation. However, a balance must be achieved to produce a dual conjugate with a sufficient number of chelators for efficient radiolabeling and which possesses enough dye molecules for an adequate imaging signal in vivo.

Several approaches, such as the development of multifunctional single-attachment point (MSAP) compounds,[13] have been designed to simplify the dual labeling process by combining optical and nuclear contrast into a single molecular moiety. The MSAP scaffold is based on functionalization of reactive peptide side chains and relies on manufacturing by solid-phase peptide synthesis (SPPS) and, thus, is limited by the range of chemistries available on the solid phase, as well as lower fluorescent labeling yields compared to those of solution-phase synthesis. Also, the use of intricate protecting group tactics on SPPS is needed, and such groups, along with the functional groups employed, need to withstand the iterative deprotection steps, which can often be harsh. In a chelator-based approach for mAb dual labeling, the BFCA diethylenetriaminepentaacetic acid (DTPA) was combined with Cy 5.5 through a lysine-based linker.[14] This approach is effective for SPECT agent development but not amenable for use with positron emitters such as ^{64}Cu or ^{68}Ga due to the selection of DTPA as a chelator. Recently, a heterofunctionalized sarcophine cage designed for ^{64}Cu labeling was used to selectively conjugate a targeting ligand and fluorescent dye, though its use with other radionuclides was not described.[15]

dx.doi.org/10.1021/jm300906g | J. Med. Chem. 2013, 56, 406−416

Synthesis of MMC Intermediates and Dye Conjugates. We developed MMC derivatives based on the tetraaza macrocyclic compound tri-*tert*-butyl 2,2′,2′′-(1,4,7,10-tetraazacyclododecane-1,4,7-triyl)triacetate (**1**) due to its similarity to DOTA. DOTA complexes have been reported for many metals, such as Gd for MRI,[16] and various radiometals for nuclear imaging.[17−19] In this study, compound **3** served as a key intermediate for synthesis of dye conjugates and was prepared by alkylation of **1** to afford **2**. Compound **2** underwent deprotection of the BOC protecting groups with concentrated HCl (Scheme 1). The compound was obtained with 90% yield, characterized by NMR and MS, and showed >95% purity on HPLC. As shown in Scheme 2, compounds **4**−**6** were synthesized by reacting **3** with IRDye 800CW−NHS, fluorescein−NHS, and CF790−NHS in sodium bicarbonate buffer (pH 8.5) at 4 °C. After isolation by semipreparative HPLC, the identity of the dye conjugates was confirmed by MS. HPLC analysis of **4** showed that the compound was obtained with >95% purity. Each compound was lyophilized, stored at −20 °C, and protected from light until further use.

Radiochemistry and Stability. To demonstrate the versatility of our MMC approach for different probe development strategies, we developed ^{68}Ga chelates that are suitable for rapidly clearing compounds, such as mAb fragments, and ^{64}Cu chelates for compounds with longer circulations times, such as full-length mAbs. The initial radiolabeling experiments used ^{68}Ga due to the presence of an in-house generator which could be eluted multiple times per day to facilitate rapid method development and optimization. Using published methods[20] with some modifications, **3**−**6** were radiolabeled with ^{68}Ga using a cation exchange column to purify and concentrate the generator eluate prior to chelation. As shown in Table 1, ^{68}Ga-labeled analogues of **3**−**5** could be obtained with radiochemical yields (RCYs) of ≥95% within 10 min and did not require further purification. Samples used for pharmacological testing had acetone removed under a stream of nitrogen and received 10−20 μL of 1 N NaOH to adjust to pH 7 or were passed through a SepPak C18 cartridge. The results indicate that the presence of IRDye 800CW and fluorescein did not affect the labeling efficiency, thus encouraging their future use with molecules which clear rapidly from the blood and can be imaged at earlier time points with ^{68}Ga PET. Interestingly, compound **6** did not label as efficiently with ^{68}Ga as the other dye conjugates even when heating times were extended to 20 or 30 min. CF790 was selected on the basis of earlier experiments which demonstrated its strong fluorescent signal before and after radiolabeling,[8] although it may not be ideal for use with this MMC analogue due to its large MW (~3200), which may interfere with incorporation of ^{68}Ga into the macrocyclic core. Also, we were not able to obtain the chemical structure of the dye to determine if it possesses functional groups that may impact radiolabeling.

Table 1. Radiolabeling Results for Compound 3 and Subsequent Dye Conjugates

compd	^{68}Ga RCY[a] (%)	^{64}Cu RCY (%)
3	95.0 ± 2.5	98.0 ± 1.0
4	95.1 ± 2.9	95.2 ± 1.2
5	99.5 ± 0.8	na[b]
6	80.9 ± 4.2	na

[a]RCY = radiochemical yield. [b]Not available.

Although DOTA does not possess the same in vivo stability as 1,4,8,11-tetraazacyclotetradecane-*N*,*N*′,*N*″,*N*‴-tetraacetic acid (TETA),[21] ^{64}Cu-DOTA complexes have nonetheless been successfully used in mAb imaging.[22,23] ^{64}Cu labeling was initially evaluated with **3** to demonstrate feasibility, and then **4** was selected as the fluorescent analogue of choice on the basis of our prior experiences with IRDye 800CW.[24−27] As with ^{68}Ga, the presence of IRDye 800CW did not impact ^{64}Cu labeling as both ^{64}Cu-**3** and ^{64}Cu-**4** could be obtained with RCY ≥ 95% (Table 1). On the basis of the radiolabeling studies, we concluded that the MMC platform could be labeled with both radiometals in high yield and that conjugation of fluorescein and IRDye 800CW to the chelator does not significantly impact the coordination chemistry.

The in vitro stability of ^{68}Ga-**4** and ^{64}Cu-**4** was assessed in mouse serum. Both agents were stable as indicated by the low amounts of free ^{68}Ga and ^{64}Cu detected by radio-HPLC. At 3 h of incubation, 97.8 ± 1% of ^{68}Ga-**4** was unchanged, while 93.7 ± 4.2% of ^{64}Cu-**4** was unchanged at 24 h. The results show that **4** forms stable coordination complexes with both ^{68}Ga and ^{64}Cu, thus enabling both radiolabeling approaches to be used for in vivo studies without concerns over demetalation.

Spectroscopic Characterization of MMC−Dye Conjugates. Varying formulations used for synthesis of dual-labeled imaging agents can impact the optical properties of a fluorophore and directly affect the image quality.[8] Table 2 shows the optical properties of IRDye 800CW- and CF790-containing compounds following chemical and radiochemical procedures. The conjugation of IRDye 800CW to **3** resulted in the formation of **4** and had a mild impact on values obtained for the extinction coefficient (EC) (8% decrease) and quantum yield (QY) (3% decrease). Conversely, ^{64}Cu labeling caused nearly a 20% decrease in both parameters, while ^{68}Ga labeling reduced the EC by nearly 35% and the QY by 24.2%. A similar trend was shown for CF790-containing agents, although the percent decrease was more substantial. The relative brightness (RB) of IRDye 800CW-containing compounds was calculated from the fluorometric assays and is shown in Figure 1A. In the preparation of **4**, the conjugation of IRDye 800CW to **3** resulted in an 11.1% decrease in the RB compared to that of unmodified IRDye 800CW. Labeling with ^{64}Cu further reduced the fluorescence intensity by 33.3% compared to the baseline value, while labeling with ^{68}Ga, which requires significantly harsher labeling conditions than ^{64}Cu, caused a 50.5% reduction in the RB. A similar pattern was observed for CF790 and its analogues (Figure 1B), although the overall decrease in the RB was greater, indicating less stability of this

Table 2. Spectral Properties of MMC−Dye Conjugates Pre- and Post-radiolabeling

compd	EC[a] (mol^{-1} cm^{-1})	QY[a]
IRDye 800CW	177 338	0.033
4	162 359	0.032
^{64}Cu-**4**	143 339	0.027
^{68}Ga-**4**	115 541	0.025
CF790	206 195	0.046
6	176 192	0.041
^{64}Cu-**6**	158 721	0.030
^{68}Ga-**6**	129 931	0.028

[a]Samples were normalized with ICG (ϕ = 0.016), λ_{ex} = 785 nm, λ_{em} = 830 nm.

dx.doi.org/10.1021/jm300906g | J. Med. Chem. 2013, 56, 406−416

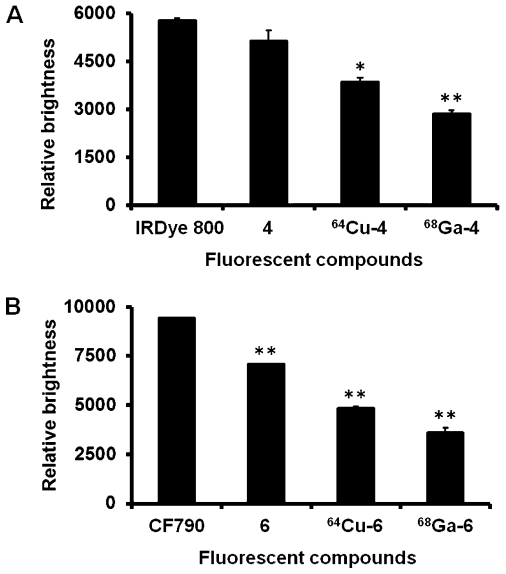

Figure 1. RB of IRDye 800CW-containing (A) and CF-790-containing (B) compounds following conjugation and radiolabeling. Data points represent the RB (EC × QY) for each compound (n = 3) following analysis of the optical properties by fluorometry. Key: *, $P < 0.005$; **, $P < 0.001$.

dye compared with IRDye 800CW. Thus, taking into account the high radiolabeling yields and optical stability, we selected the IRDye 800CW-based compound **4** for further characterization.

In Vivo Characterization of Radiolabeled Analogues of 4 in Normal Mice. To assess the in vivo distribution of ^{68}Ga-**4** and ^{64}Cu-**4**, multimodality imaging studies were performed in normal mice and the data was compared to mice receiving control agents: ^{68}Ga-DOTA, ^{64}Cu-DOTA, and IRDye 800CW. First, dynamic PET imaging was conducted in mice after iv injection of each radioactive agent. Time−activity curves (TACs) were generated for the liver, kidney, muscle, heart, and bladder to monitor distribution and PK. As shown by selected TACs in Figure 2, activity in the heart reached a peak within 2 min postinjection (pi) and exhibited a nearly 3-fold increase in percent injected dose per gram of tissue (%ID/g) for ^{64}Cu-**4** versus ^{68}Ga-**4**. Uptake values for both agents declined gradually but remained higher than the background (i.e., muscle) levels. Analysis of the corresponding ^{64}Cu- and ^{68}Ga-DOTA controls revealed similar kinetic profiles, suggesting rapid removal of ^{64}Cu-**4** and ^{68}Ga-**4** from the blood upon first pass distribution in the body. For ^{64}Cu-**4**, the bladder showed the highest radioactivity, which rose sharply within 10 min and then remained constant for the duration of the imaging session. The bladder was also the highest site of ^{68}Ga-**4** levels, though accumulation was more gradual. The rapid excretion through the urine was consistent with other reports on nontargeted macrocyclic BFCAs[28,29] and with bladder uptake of 50.84%ID/g for ^{64}Cu-DOTA at 10 min and 39.78% ID/g for ^{68}Ga-DOTA at 16 min (data not shown). MMC conjugates had lower kidney uptake than their DOTA counterparts, likely due to the increase in MW and reduced hydrophilicity incurred by conjugation with IRDye 800CW. Kidney uptake for ^{68}Ga-**4** reached a peak of 5.05%ID/g at 3 min pi and then decreased over the course of the study, while ^{64}Cu-**4** reached a similar activity level within 2 min pi but showed a moderate increase over time. This difference may be explained by the somewhat limited in vivo stability of ^{64}Cu-DOTA complexes and structural mimics of DOTA (e.g., MMC), which results in transchelation of ^{64}Cu to serum proteins and higher blood pool activity.[21] The elevated radioactivity levels in the blood may act as a constant source of agent for the kidneys at early time points and contribute to the observed differences in kidney uptake of ^{64}Cu-**4** and ^{68}Ga-**4**. Previous reports by our group and others suggest that prolonged retention of radioactivity in the blood due to ^{64}Cu transchelation may also contribute to a higher liver signal compared to that of ^{68}Ga-labeled counterparts.[30−32] Our observations from the current study are in agreement with those findings as approximately 5-fold higher ^{64}Cu-**4** activity

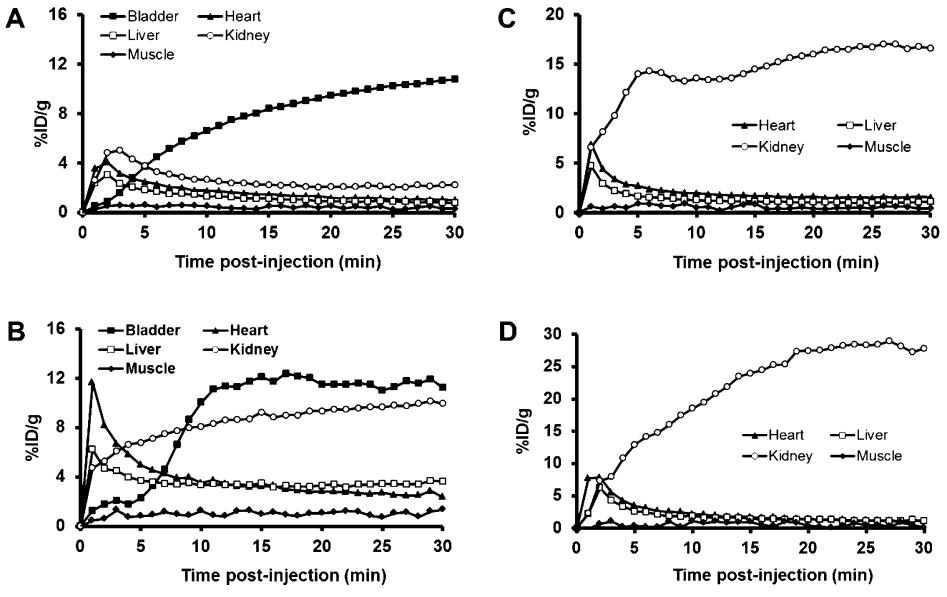

Figure 2. Time−activity curves of selected tissues generated from dynamic PET imaging with ^{68}Ga-**4** (A), ^{64}Cu-**4** (B), ^{68}Ga-DOTA (C), and ^{64}Cu-DOTA (D).

dx.doi.org/10.1021/jm300906g | J. Med. Chem. 2013, 56, 406−416

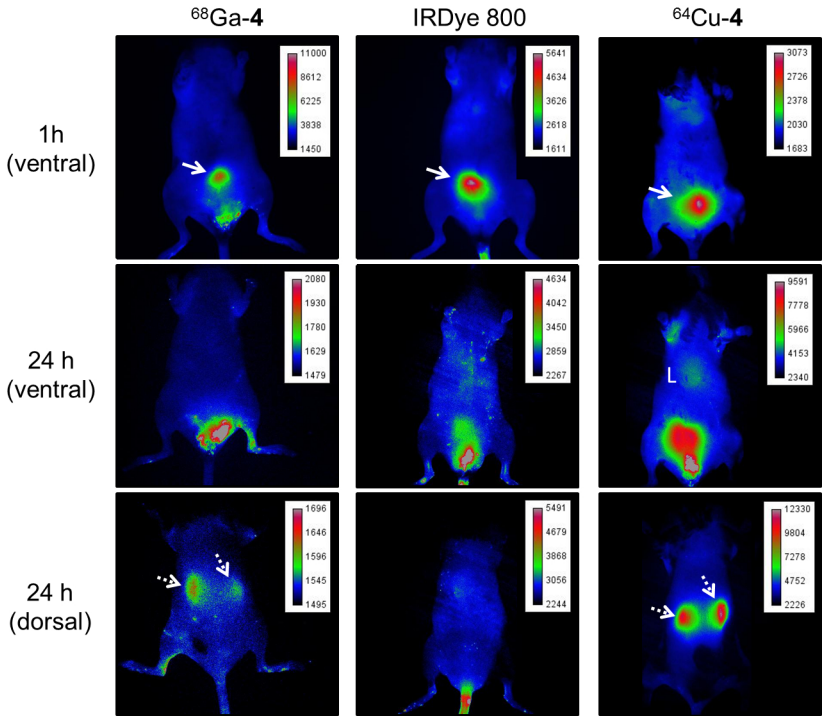

Figure 3. NIRF images of tumor-free mice obtained 1 and 24 h postinjection of ^{68}Ga-**4** (left), IRDye 800CW (center), and ^{64}Cu-**4** (right). Bladder (solid arrows) and kidney (dashed arrows) uptake are visualized in ventral and dorsal views, respectively. Liver (L) uptake of ^{64}Cu-**4** is visible at 24 h. Different scales are shown for each image, and in the case of ^{68}Ga-**4**, the intensity scale range at 24 h has a maximum value slightly above background levels, indicating nearly complete clearance of the agent from the body.

was present in the liver compared with that of ^{68}Ga-**4** at 30 min pi.

In vivo NIRF imaging of ^{68}Ga-**4** and ^{64}Cu-**4** was conducted after completion of the PET scans, and the images were compared to those obtained for administration of an equimolar dose of IRDye 800CW alone. Signal was primarily seen in the bladder and kidneys, consistent with the expected renal clearance route. Compared to IRDye 800CW, ^{68}Ga-**4** showed greater bladder accumulation at 1 h, while ^{64}Cu-**4** was more slowly cleared (Figure 3). At 24 h, ventral and dorsal views show that ^{68}Ga-**4** was nearly completely removed from the body. Conversely, the ^{64}Cu-**4** signal was well above background at 24 h and showed high levels of agent in the bladder and kidneys, along with increased contrast in the liver. These findings support the PET data indicating that ^{68}Ga-**4** is passively distributed through tissues at early time points and undergoes rapid renal clearance and elimination from the body, whereas ^{64}Cu-**4** experiences extended circulation which involves both renal and hepatobiliary clearance routes commonly associated with many ^{64}Cu radiopharmaceuticals. From the multimodal imaging studies, we concluded that the PK properties of **4** are in accordance with conventional, non-targeted BFCAs and, thus, well-suited for in vivo imaging. Furthermore, the efficient clearance from normal tissues suggests that, upon coupling with a targeting agent, **4** will not contribute significantly to nonspecific binding, thus promoting enhanced contrast and target visualization.

To examine the tissue distribution of **4** and quantify nonspecific organ uptake, biodistribution studies were conducted in tumor-free mice injected with ^{64}Cu-**4** and are summarized in Figure 4. Consistent with the dynamic PET data, the highest radioactivity concentration was found in the urine at 1 h pi (data not shown). Accumulation of ^{64}Cu-**4** at 1 h

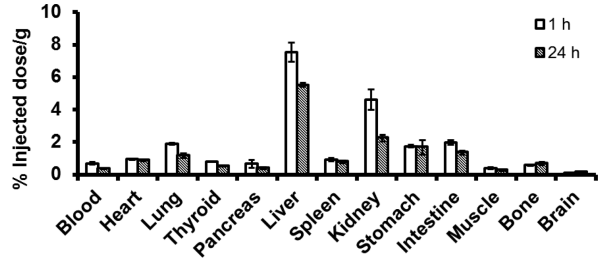

Figure 4. Biodistribution of ^{64}Cu-**4** in normal nude mice.

pi was predominantly in the liver and kidneys (7.53 ± 0.58% ID/g and 4.6 ± 0.63%ID/g, respectively), with minor signal in the lungs, stomach, and intestine. Uptake in the kidneys was sharply reduced from 1 to 24 h pi (51.3% decrease), whereas liver activity incurred less of a reduction (26.8%) over the same period, likely due to transchelation of ^{64}Cu to copper-binding enzymes in the liver.[33] Low levels of blood activity were observed at both time points (0.7 ± 0.07%ID/g and 0.36 ± 0.04%ID/g at 1 and 24 h, respectively) presumably due to the small size and polar characteristics of the compound, while also indicating limited transchelation of ^{64}Cu by serum proteins. On the basis of the biodistribution results, low levels of nonspecific binding were observed, indicating that **4** does not actively target normal tissues and is unlikely to affect the biological activity of a targeting ligand after conjugation.

Synthesis and Radiolabeling of 7. To evaluate the conjugation of **4** to mAbs, model conjugation studies were performed with a custom EpCAM-targeting mAb developed in-house.[34] To prepare MMC immunoconjugate **7**, **4** was mixed with sulfo-NHS and *N*-(3-(dimethylamino)propyl)-*N*′-ethyl-carbodiimide (EDC) in water and then added to a solution of mAb7 in sodium phosphate dibasic buffer, pH 8.5 (Scheme 3).

dx.doi.org/10.1021/jm300906g | *J. Med. Chem.* 2013, 56, 406−416

Scheme 3. Synthesis of MMC-Functionalized Immunoconjugate 7[a]

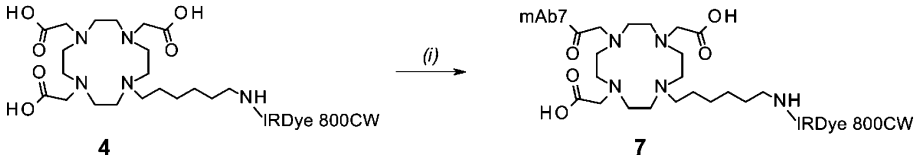

[a]Reagents and conditions: (i) EDC, sulfo-NHS, H_2O, Na_2HPO_4 (0.1 M, pH 8.5), mAb7, 4 °C, overnight.

After reaction overnight, the product was purified by gel filtration chromatography and analyzed by size-exclusion HPLC. Traces were obtained at 280 nm for identification of the mAb and at 780 nm to detect the presence of IRDye 800CW as a component of **4**. Compound **7** had a retention time of 7.6 min at 280 nm with a corresponding 780 nm peak at 7.6 min, suggesting successful conjugation. On size-exclusion HPLC, **4** eluted at 11.5 min and <1% was present after purification of **7**.

Compound **7** was labeled with ^{64}Cu at pH 6 in 0.1 N sodium acetate and resulted in a RCY of 51.9% based on 100 μg/mCi. After gel filtration chromatography, the product was >95% pure and was directly used for pharmacological assays. Using similar reaction conditions, the isotype control mAb **8** was ^{64}Cu-labeled with 78.2% RCY and showed >97% purity after purification.

Determining the Number of Chelates per mAb and Immunoreactivity. Quantification of the ratio of MMC moieties per mAb was assessed by carrier-added radiolabeling with ^{64}Cu and fluorescence spectrophotometry, allowing cross-validation of the findings. Using a 50-fold excess of **4**, compound **7** was prepared with 1 chelator per mAb. Compound **8** was prepared with 2.8 chelators per mAb due to excess **4** used in the reaction. Such low conjugation ratios are not expected to hamper the specific binding affinity, and indeed, this was confirmed through in vitro studies using PC3-DsRed cells which overexpress EpCAM. From flow cytometry experiments, detection on the NIR channel showed the mean number of cells stained with **7** was 80.8% with a median fluorescence intensity (MFI) of 1722 compared to 599 for unstained cells (Figure 5). The data suggest that conditions for synthesizing **7** do not result in overmodification of the mAb and preserve specific binding capabilities. In addition, the chelator:protein ratio obtained permits sufficient RCY with a strong fluorescence signal also being exhibited. On the basis of the standard coupling conditions used, these methods could be applied for kit-based preparation with other mAbs intended for dual labeling.

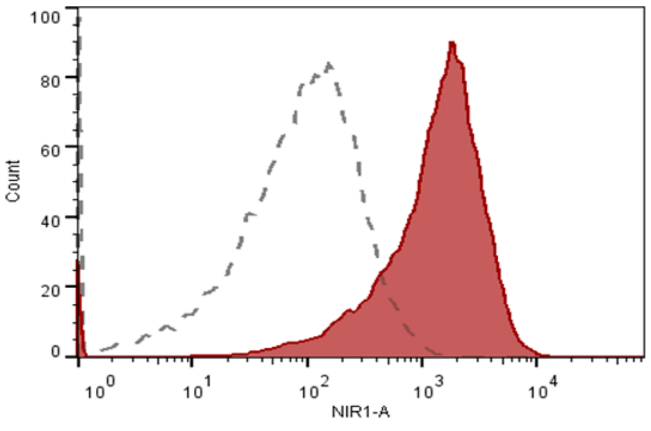

Figure 5. Flow cytometry analysis. Compound **7** was added to PC3-DsRed cells and sorted using a customized flow cytometer with NIR excitation and emission detection capability. A histogram from a representative reaction is shown, demonstrating a shift in the cell population after staining with **7**.

Cell-Binding Assays. In vitro uptake of ^{64}Cu-**7** was evaluated in PC3-DsRed cell lines known to express EpCAM and is summarized in Figure 6. ^{64}Cu-**8** (isotype control mAb) and ^{64}Cu-**4** (nontargeted) were used as controls. The 1 h incubation time point showed higher ^{64}Cu-**7** uptake (4.64 ± 0.22% of the total radioactivity added) compared to that of the controls (<0.97%). Increased uptake of ^{64}Cu-**7** was observed as a function of time and reached 21.09 ± 0.24% of total radioactivity added at 24 h. Since experiments were carried out at 37 °C, the radioactivity counted likely represented a combination of cell-bound and internalized agent and requires further analysis by fluorescence microscopy to determine binding/internalization properties of the agent. The in vitro findings indicated that conjugation of **4** to mAb7 results in a bioactive immunoconjugate that can bind to EpCAM in prostate cancer cell lines. Also, the data show that ^{64}Cu-**4** does not actively associate with tumor cells and is unlikely to contribute to the uptake observed with an MMC conjugate, further enhancing its value as a novel chelator for dual-labeled probe development.

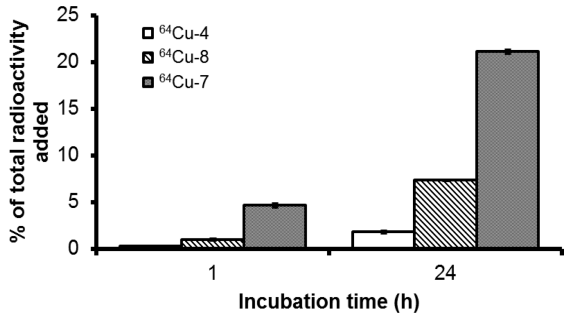

Figure 6. In vitro uptake of ^{64}Cu-**7** in PC3-DsRed cells. Data points represent the percentage of total activity added ± SD and were obtained in triplicate. ^{64}Cu-**4** and ^{64}Cu-**8** were used as controls.

In Vivo Characterization in Tumor-Bearing Mice. Multimodality imaging studies were performed to assess the tumor-targeting capabilities of ^{64}Cu-**7** in mouse xenografts. PC3 cells transfected with the DsRed reporter have been used by our group to noninvasively track tumor formation, growth, and metastases by optical imaging.[12,34] Accordingly, we employed PC3-DsRed cells to serve as "ground truth" for interpretation of NIRF and PET imaging results. As shown in Figure 7, the tumor was very small at the time of the imaging experiments (~4.5 mm) but was easily detected by DsRed and NIRF imaging owing to the submillimeter resolution of these

dx.doi.org/10.1021/jm300906g | J. Med. Chem. 2013, 56, 406−416

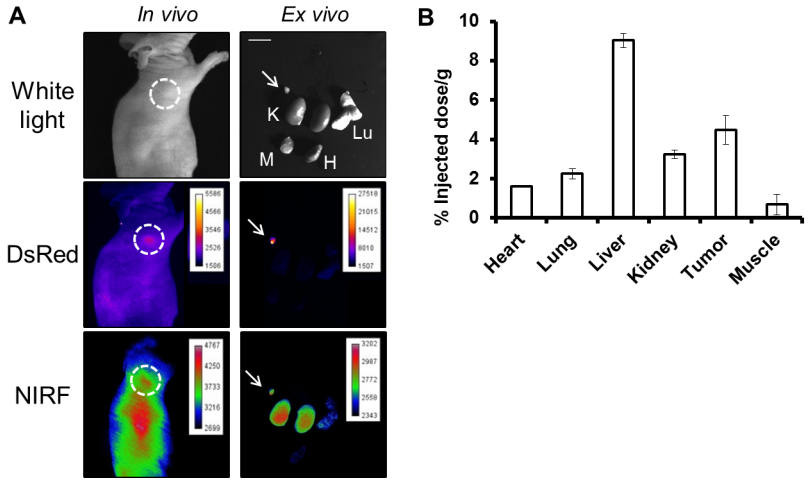

Figure 7. Representative multimodality images in a tumor-bearing mouse 40 h postinjection of ^{64}Cu-**7** (A). The focal tumor signal was visualized by DsRed and NIRF imaging in vivo (circle). Ex vivo imaging on selected tissues showed comparable fluorescence levels in the kidneys and tumor with low signal elsewhere. Quantification of ^{64}Cu-**7** uptake is represented in (B) and indicates the highest signal in the liver, tumor, and kidneys. The arrow indicates the excised tumor. K = kidney, Lu = lung, H = heart, and M = muscle. The scale bar represents 1.6 cm.

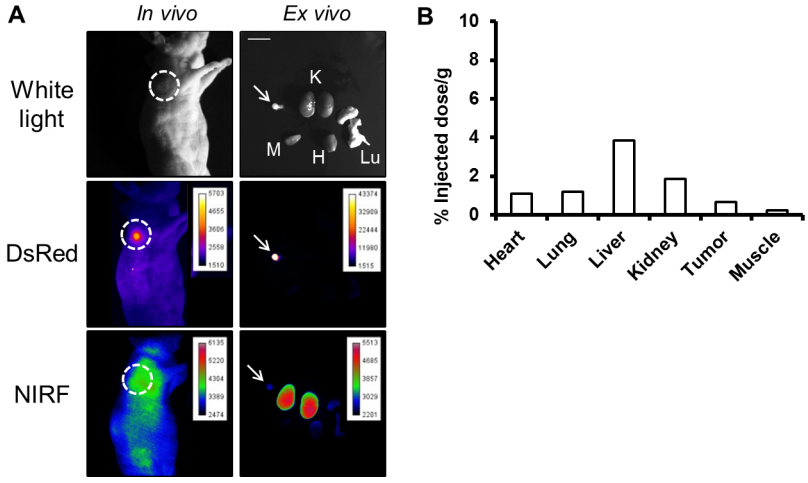

Figure 8. Representative multimodality images in a tumor-bearing mouse 40 h postinjection of ^{64}Cu-**4** (A). In vivo DsRed imaging revealed an intense, focal fluorescent signal corresponding to the tumor site that was not clearly delineated by NIRF (circle). Ex vivo imaging on selected tissues showed high fluorescence levels in the kidneys with low signal elsewhere. Quantification of ^{64}Cu-**4** uptake is represented in (B) and indicates the highest signal in the liver and kidneys, with low accumulation in other tissues. The arrow indicates the excised tumor. K = kidney, Lu = lung, H = heart, and M = muscle. The scale bar represents 1.6 cm.

modalities.[35] However, the small size of the tumor made visualization by whole-body μPET/CT challenging and necessitated ex vivo analysis to better assess the imaging properties of ^{64}Cu-**7**. Tumors and other tissues were excised at 40 h pi and underwent DsRed and NIRF imaging, followed by quantification of radioactivity with a γ counter. Using NIRF imaging, we found fluorescent signal in the tumor which correlated with the DsRed signal and also observed agent uptake in the liver and kidneys with minimal signal in other tissues. The NIRF findings were further supported by quantification of radioactivity which showed 4.48 $\pm$ 0.75% ID/g in the tumors in addition to expected clearance through the liver (9.03 $\pm$ 0.36%ID/g) and kidneys (3.25 $\pm$ 0.22%ID/g). In mice receiving ^{64}Cu-**4**, whole-body NIRF imaging did not clearly identify the tumor site and instead showed a diffuse signal (Figure 8). After excision of tissues, we found tumor uptake of ^{64}Cu-**4** to be 1.26 $\pm$ 0.84%ID/g with notable accumulation in the liver (4.39 $\pm$ 0.75%ID/g) and kidneys (2.07 $\pm$ 0.29%ID/g). Tumor imaging studies confirmed the nontargeting characteristics of ^{64}Cu-**4** while showing that its conjugation to a target-specific mAb enabled tumor-associated contrast. Moreover, the lack of tumor uptake by **4**, coupled with its low levels in background tissues shown by biodistribution studies and NIRF imaging, encourages further development and optimization of the MMC scaffold for dual-labeled mAb development.

Our findings, along with the growing interest in hybrid agent development, encourage the use of multimodality imaging as a means to improve agent characterization by capitalizing on the respective strengths of each imaging technology. NIRF imaging enabled visualization of very small tumors that would have otherwise been missed by PET alone, while the presence of the radiolabel enhanced the NIRF data by providing quantifiable tissue distribution and cross-validation. Further improvements in agent design that incorporate bio-orthogonal conjugation strategies will remove concerns regarding overmodification of

dx.doi.org/10.1021/jm300906g | J. Med. Chem. 2013, 56, 406−416

mAbs with NHS-based dual labeling and promote product homogeneity. For example, regioselective conjugation approaches, such as reduction of interchain disulfides on mAbs for alkylation with maleimide-based agents,[36] would place MMC (or other) moieties at conjugation sites that are distant from the pharmacophore and produce more potent immunoconjugates. Furthermore, this strategy would promote batch-to-batch reproducibility and minimize concerns over agent design and variability that affect interpretation of pharmacological data and translational potential. Bio-orthogonal tactics have also been used with the highly selective and rapidly occurring inverse-electron-demand Diels–Alder reaction for tumor pretargeting with radiolabeled mAbs.[37] Exquisite sensitivity for target tissues was achieved in mice with pronounced localization of radioactivity in the tumor as demonstrated by SPECT imaging. Efforts to integrate these innovative methods into dual labeling scaffolds are feasible and would likely improve imaging capabilities, manufacturing practices, and validation methods.

CONCLUSIONS

In summary, we have developed an MMC scaffold based on a versatile macrocyclic backbone which permits chelation of radiometals with biomedical applications and conjugation to NIRF dyes and targeting molecules. Our strategy to simplify the dual labeling of mAbs builds upon the growing interest in fluorescent imaging techniques for surgical guidance and also carries the advantages of nuclear imaging, which is a standard-of-care modality in several diseases. Nontargeted MMC–dye conjugates showed efficient radiolabeling, sufficient optical stability, rapid clearance, and low levels of uptake in normal tissues in mice. Conjugation of **4** to an EpCAM-specific mAb demonstrated a simple dual labeling approach as evidenced by the low number of MMC moieties per mAb, retention of immunoreactivity, and reasonable labeling yields with ^{64}Cu. Binding assays confirmed targeting capabilities in prostate cancer cells, and tumor imaging studies revealed excellent correlation among endogenous tumor fluorescence, targeted NIRF signal, and quantification of radioactivity.

With the MMC scaffold, the combination of a chelator and dye into a single molecule reduces the conjugation footprint by half compared to conventional dual labeling methods. Hence, there is less chance for overmodification of a mAb and interference with its binding domain. This is of particular significance with antibody fragments where there is limited real estate for conjugation and increased risk for disrupting biological activity. Upon continued optimization and validation, such a scaffold may potentially become a reagent for simple, kit-based preparation of dual-labeled agents and support the translation of promising fluorescence-based agents into the clinic.

EXPERIMENTAL SECTION

General Procedures. All reagents and solvents were analytical grade, were purchased from commercial suppliers, and were used without further purification unless otherwise stated. Chelex-100 resin was purchased from Bio-Rad Laboratories (Richmond, CA) and used with all aqueous buffers to ensure metal-free conditions. Tri-*tert*-butyl 2,2′,2′′-(1,4,7,10-tetraazacyclododecane-1,4,7-triyl)triacetate was purchased from Macrocyclics (Dallas, TX). IRDye 800CW-NHS was purchased from Li-COR Bioscience (Lincoln, NE). CF790-NHS was purchased from Biotium (Hayward, CA). A 30 mCi ^{68}Ge/^{68}Ga generator was purchased from Eckert & Ziegler (Berlin, Germany). ^{64}Cu was produced by the Washington University School of Medicine (St. Louis, MO). *Caution: Due to the positron and γ-ray emissions of ^{68}Ga and ^{64}Cu, it is imperative that individuals following these procedures observe the guidelines set forth by their institution and use proper protective equipment and shielding when handling any radioactive materials!* ^{1}H NMR and ^{13}C NMR spectra were recorded at ambient temperature using 300 and 600 MHz IBM-Bruker Avance NMR spectrometers. Chemical shifts (δ) were reported (ppm) downfield of tetramethylsilane. Low-resolution ESI mass spectra were acquired on an LCQ FLEET instrument (Thermo Scientific) in our laboratory. Final nonradioactive compounds were purified to ≥95% as determined by the elution of single peaks on HPLC. For the low-MW MMC derivatives, RP-HPLC was performed on an analytical and semi-preparative Hitachi LaChrom system using Ultra C18 (5 μm) columns (Hitachi) with mobile phases of A = 0.1% TFA in H_2O and B = 0.1% TFA in CH_3CN (gradient: 0 min, 10% B; 15 min, 90% B) and a flow rate of 1 mL/min. MMC–mAb conjugates were analyzed using size-exclusion chromatography with a TSKgel G3000SW (5 μm) column and mobile phases of A = 0.1 M sodium phosphate buffer (pH 7.3) and B = CH_3CN (isocratic (90% A and 10% B)) and a flow rate of 1 mL/min. Radiochemical purities of ≥95% were assessed by (1) radio-TLC with Whatman chromatography paper and 0.1 M ammonium acetate/0.05 M EDTA (pH 6) as the mobile phase with analysis using an AR-2000 scanner (Bioscan) and (2) radio-HPLC using an in-line radioactive detector (Berthold Technologies).

Synthesis of *tert*-Butyl 2,2′,2″-(10-(*N*-(*tert*-butoxycarbonyl)-6-aminohexyl)-1,4,7,10-tetraazacyclododeca-1,4,7-triyl)-triacetate (2). Compound **1** (250 mg, 0.48 mmol) and potassium carbonate (138 mg, 1.0 mmol) in 10 mL of anhydrous acetonitrile were stirred at room temperature for 30 min. To the solution was added 6-((*tert*-butoxycarbonyl)amino)hexyl bromide (130 mg, 0.48 mmol), and the resulting mixture was heated at 70 °C overnight. The reaction mixture was filtered and evaporated under reduced pressure and purified by silica gel column chromatography (4% methanol in CH_2Cl_2, v/v) to give **2** (235 mg, 67%). ^{1}H NMR ($CDCl_3$, 600 MHz): δ (ppm) 1.44 (s, 36H), 1.45–1.72 (m, 8H), 2.78–3.65 (m, 26H), 4.68 (br, 1H). ^{13}C NMR ($CDCl_3$, 600 MHz): δ (ppm) 23.09, 26.08, 27.81, 29.74, 40.27, 47.78, 50.29, 52.74, 53.04, 55.51, 56.92, 78.97, 81.83, 156.04, 169.93. ESI-MS (m/z): calcd, 713.53; found, 714.3 $(M + H)^+$.

Synthesis of 2,2′,2″-(10-(6-Aminohexyl)-1,4,7,10-tetraazacyclododeca-1,4,7-triyl)triacetic Acid (3). A solution of **2** (200 mg, 0.28 mmol) in 6 mL of concentrated HCl (34–37%) was stirred at room temperature for 4 h. The reaction mixture was evaporated under reduced pressure, and the resulting gummy residue was dissolved in H_2O and lyophilized to afford **3** as a white solid (118 mg, 94%). ^{1}H NMR (D_2O, 600 MHz): δ (ppm) 1.67–1.90 (m, 8H), 2.88–3.53 (m, 26H), 4.14 (s, 1H). ^{13}C NMR ($CDCl_3$, 600 MHz): δ (ppm) 22.78, 25.13, 25.23, 26.42, 39.31, 47.95, 48.42, 49.88, 51.94, 52.91, 54.29, 54.65, 170.00, 174.31. ESI-MS (m/z): calcd, 445.29; found, 446.2 $(M + H)^+$, 468.2 $(M + Na)^+$.

Synthesis of 2,2′,2″-(10-(6-IRDye 800CW hexyl amide))-1,4,7,10-tetraazacyclododeca-1,4,7-triyl)triacetic Acid (4). To a stirred solution of **3** (500 μg, 1.1 μmol) in 1 mL of sodium bicarbonate buffer (pH 8.5) was added IRDye 800CW–NHS ester (2 mg, 0.85 μmol) dissolved in DMSO (500 μL). The reaction mixture was stirred for 18 h at room temperature and protected from light. Solvent was removed under reduced pressure, and the residue was purified by semipreparative HPLC. After lyophilization, **4** was obtained as a green solid (1.4 mg, 80%). Compound **4** was characterized by NMR and ESI-MS spectroscopy. ^{1}H NMR (D_2O, 600 MHz): δ (ppm) 1.16–1.90 (m, 32H), 2.09 (t, J = 6.6 Hz, 2H), 2.61(m, 4H), 2.86 (t, J = 7.2 Hz, 2H), 2.91 (t, J = 7.2 Hz, 2H), 3.26–3.40 (m, 26 H), 3.9–4.0 (m, 4H), 6.08–6.12 (dd, J = 10.2, 3.6 Hz, 2H), 7.19 (d, J = 9 Hz, 4H), 7.69 (m, 4H), 7.76 (m, 4H). The detected molecular ions were consistent with the exact mass of $C_{66}H_{91}N_7O_{20}S_4$ (1429.52). ESI-MS (+) (m/z): found, 1430.3 $(M + H)^+$, 715.2 $(M + H)^{2+}$.

Synthesis of 2,2′,2″-(10-(6-Fluorescein hexyl amide))-1,4,7,10-tetraazacyclododeca-1,4,7-triyl)triacetic Acid (5). Compound **5** was prepared using the same procedure as that used for **4**. To a solution of **3** (5 mg, 11 μmol) in sodium bicarbonate buffer (2 mL) was added fluorescein–NHS (5.3 mg, 11 μmol) in DMSO (2

dx.doi.org/10.1021/jm300906g | J. Med. Chem. 2013, 56, 406–416

mL) to afford **5** (6.9 mg, 76%). ^{1}H NMR (D_2O, 600 MHz): δ (ppm) 1.49 (s, 27H), 1.56−1.90 (m, 8H), 2.00−3.8 (m, 26H), 5.41 (s, 1H), 6.5−6.7 (m, 6H), 7.31 (s, 1H), 8.1 (s, 1H), 8.2−8.4 (m, 2H). The detected molecular ions were consistent with the exact mass of $C_{41}H_{49}N_5O_{12}$ (803.33). ESI-MS (+) (m/z): found, 804.3 $(M + H)^+$, 402.7 $(M + H)^{2+}$.

Synthesis of 2,2′,2″-(10-(6-CF790 hexyl amide))-1,4,7,10-tetraazacyclododeca-1,4,7-triyl)triacetic Acid (6). Compound **6** was prepared using the same procedure as that used for **4**. To a solution of **3** (500 μg, 1.1 μmol) in sodium bicarbonate buffer (0.5 mL) was added CF790−NHS (1.6 mg, 0.5 μmol) in DMSO (0.5 mL) to afford **6** (1.4 mg, 80%). Compound **6** was characterized by HPLC.

Radiochemistry. ^{68}Ga labeling was conducted using the method of Zhernosekov et al.[20] with modifications. Briefly, the ^{68}Ge/^{68}Ga generator was eluted with 5 mL of 0.1 M HCl and the radioactivity was adsorbed onto a Strata-X cation exchange cartridge. The cartridge was dried with an air purge, and ^{68}Ga (37−74 MBq) was collected with 98% acetone/0.02 M HCl (v/v) and added to 20 nmol of each sample in 0.2 M sodium acetate (pH 4). Complexation was carried out at 95 °C for 10 min with analysis by radio-HPLC.

Compound **4** was selected for further radiolabeling studies using ^{64}Cu. A 37−74 MBq solution of $^{64}CuCl_2$ was added to compound **4** (20 nmol) in 0.1 M sodium acetate (pH 6) and heated at 50 °C for 1 h. The purity was assessed by radio-HPLC. ^{64}Cu-**4** was diluted in PBS and passed through a 0.22 μm syringe filter for in vivo studies.

Stability Studies. The in vitro stability of ^{68}Ga-**4** and ^{64}Cu-**4** was evaluated in 50% mouse serum (Sigma-Aldrich) at 37 °C. Multiple samples were taken during 3 and 24 h incubation periods for ^{68}Ga-**4** and ^{64}Cu-**4**, respectively. Serum proteins were precipitated and filtered, and the filtrate was analyzed by radio-HPLC as previously described.[31]

Assessment of Spectral Properties. To determine the impact of chemical and radiochemical syntheses on the optical properties of IRDye 800CW, spectral analysis was performed using published methods.[8] Briefly, absorbance of all solutions was measured at 785 nm to obtain an extinction cross section from the slope of absorbance versus dye concentration. The fluorescent properties of the solutions were evaluated at $\lambda_{ex}/\lambda_{em}$ = 785/830 nm to compute the EC and QY (ϕ) using the method of Williams et al.,[38] with indocyanine green (ICG) (ϕ = 0.016) at $\lambda_{ex}/\lambda_{em}$ = 785/830 nm serving as a standard.[39] The RB of each sample was calculated as the product of the respective EC and QY values.

In Vivo Imaging and Biodistribution of Radiolabeled 4 in Normal Mice. All animal studies were performed in accordance with the standards of the University of Texas Health Science Center at Houston (Houston, TX), Department of Comparative Medicine and Center for Molecular Imaging, after review and approval of the protocol by the Institutional Animal Care and Use Committee or Animal Welfare Committee. For all imaging procedures, mice were anesthetized with 1% isoflurane. A murine model of C57BL/6 mice was used to evaluate the distribution and clearance profile of ^{68}Ga-**4** and ^{64}Cu-**4**. ^{68}Ga-DOTA and ^{64}Cu-DOTA were used as controls for PET studies. Mice were shaved one day before each imaging study to minimize light scattering effects during NIRF imaging. After a CT scan for attenuation correction, the mice (n = 3/agent) were moved into the PET field of view and injected with 5.55−7.4 MBq of agent iv. Dynamic PET imaging was performed in list mode for 30 min with a Siemens Inveon μPET/CT scanner (Siemens Medical, Knoxville, TN) using instrument parameters described elsewhere.[10] Region of interest (ROI) analysis was performed on the cumulative 30 min scan with the vendor software package (Inveon Research Workplace [IRW]) to obtain the %ID/g values for selected organs. The acquired data were sorted into 120 frames (15 s/frame) to determine the distribution and clearance profiles of the agents using the kinetic analysis feature in IRW, and TACs were generated for selected organs.

Following PET/CT imaging with ^{68}Ga-**4** and ^{64}Cu-**4**, NIRF images were acquired at 1, 4, and 24 h pi using a custom-built fluorescence imaging system previously described.[24] Mice were imaged with an exposure time of 200 ms in prone and supine positions. Image analysis was performed with the ImageJ software package (NIH, Bethesda, MD).

Normal female athymic nude mice, 4−6 weeks old, were used to evaluate the tissue distribution of ^{64}Cu-**4**. Mice were injected with 740 kBq of ^{64}Cu-**4** via the tail vein and were euthanized 1 and 24 h after injection. Organs of interest were excised, weighed, and counted in a γ counter. The results are expressed as %ID/g and represent the mean ± SD of n = 3 mice/time point. The total injected activity per mouse was determined from a known aliquot of the injected solution.

Synthesis of Immunoconjugates 7 and 8. To prepare **7**, **4** (400 μg, 280 nmol) was dissolved in 250 μL of water and then added to 100 μL of freshly prepared aqueous sulfo-NHS solution (70 μg, 320 nmol), followed by the addition of 100 μL (54 μg, 280 nmol) of freshly prepared aqueous EDC, all in ice cold conditions. After 45 min, 50 μL of sodium phosphate dibasic buffer solution (0.1 M, pH 8.5) was added to the reaction mixture, and the pH was confirmed at 8.5. To this solution was added 1 mg (6.7 nmol) of a custom mAb specific for human EpCAM[34] (referred to as mAb7) in 200 μL of sodium phosphate dibasic buffer solution (0.1 M, pH 8.5). The reaction mixture was incubated at 4 °C for 20 h with continuous end-over-end mixing. The reaction was purified with a Zeba spin desalting column, collected in PBS, and stored at −80 °C. Preparation of the isotype control mAb **8** was carried out with a 100-fold excess of **4** using the same reaction conditions.

Determination of the Number of Chelates per mAb Molecule. The number of MMC moieties per mAb molecule was calculated using a molar excess of carrier-added ^{64}Cu as previously described.[12] Since the ratio of chelator to dye is 1:1, the number of chelating groups conjugated was expected to also represent the number of dye molecules present. To confirm this, we employed our previous spectrophotometric method for determining the dye:protein ratio, which measured the absorbance of the conjugate at 780 and 280 nm using a Beckman Coulter DU 800CW UV/vis spectrophotometer (Beckman Coulter, Inc.).[12]

Flow Cytometry. PC3 cells were transfected with p-DsRedExpress-N1 (Clontech Laboratories, Inc., Mountain View, CA).[12] The immunoreactivity of MMC−mAb conjugates was determined by monitoring their ability to bind EpCAM expressed on the surface of PC3-DsRed cells[40] (ATCC, Manassas, VA) by NIR flow cytometry as previously described.[41] A customized BD FACSAria II capable of NIR detection was utilized for data acquisition and analysis. Binding of **7** was performed in triplicate and recorded as a percentage of stained cells and MFI.

Radiolabeling of Immunoconjugates. Radiolabeling of MMC−mAb conjugates was performed by adding 37 MBq of ^{64}Cu to 100 μg of **7** or **8** in 0.1 M sodium acetate (pH 6.0), followed by incubation at 40 °C for 1 h. Reactions were quenched by the addition of 3 μL of 10 mM EDTA and purified with Zeba spin desalting columns using PBS as the eluent. Each sample was analyzed by radio-TLC and radio-HPLC.

In Vitro Binding Assays. PC3-DsRed cells were cultured in Dulbecco's minimal essential medium F-12 with 10% fetal bovine serum (FBS) and G418 (640 μg/mL) at 37 °C with humidity and 5% CO_2. For the in vitro uptake assays, cells were seeded in 12-well plates (150 000 cells/well) and incubated at 37 °C for 48 h. Prior to the uptake studies, growth medium was removed and the cells were washed twice with PBS. To each well was added 1 mL of RPMI (without FBS) containing 37−74 kBq of each agent, and the plates were incubated at 37 °C for 1, 4, and 24 h. At each time point, the medium was removed and the cells were washed three times with PBS. The cells were trypsinized and collected in 1 mL of PBS, followed by measurement of the bound radioactivity by a γ counter. Each experiment was performed in triplicate, and the data were reported as percentages of total activity added.

In Vivo Imaging in Tumor-Bearing Mice. PC3-DsRed cells (1×10^6) were subcutaneously implanted in the right flank near the shoulder region of 4−6 week old male, athymic, nude mice. Longitudinal DsRed imaging was performed at $\lambda_{ex}/\lambda_{em}$ = 568/610 nm to detect fluorescent PC3 cells and monitor tumor growth as previously described.[12] Two weeks postimplantation, ^{64}Cu-**4** and ^{64}Cu-**7** were iv injected into the mice (7.4 MBq/mouse), and PET/CT and NIRF images were acquired 1, 20, and 40 h postinjection. At the

dx.doi.org/10.1021/jm300906g | J. Med. Chem. 2013, 56, 406−416

conclusion of the study, the mice were sacrificed and selected tissues were excised and imaged to examine correlation between NIRF and DsRed signals. γ counting was performed on the tissues to quantify % ID/g for each agent.

AUTHOR INFORMATION

Corresponding Author

*Phone: (713) 500-3577. Fax: (713) 500-0319. E-mail: ali.azhdarinia@uth.tmc.edu.

Notes

The authors declare no competing financial interest.

ACKNOWLEDGMENTS

We thank Otis Hall and Dr. Amy Hazen for their assistance with the flow cytometry studies. This work was supported in part by NIH Grant U54 CA136404 (E.M.S.-M.) and the Wilson Foundation (E.M.S.-M.).

ABBREVIATIONS USED

%ID/g, percent injected dose per gram; BFCA, bifunctional chelating agent; DOTA, 1,4,7,10-tetraazacyclododecane-*N*,*N*′,*N*″,*N*‴-tetraacetic acid; DTPA, diethylenetriaminepentaacetic acid; EC, extinction coefficient; EDC, *N*-(3-(dimethylamino)propyl)-*N*′-ethylcarbodiimide; EpCAM, epithelial cell adhesion molecule; FBS, fetal bovine serum; ICG, indocyanine green; IRW, Inveon Research Workplace; mAb, monoclonal antibody; MFI, median fluorescence intensity; MMC, multimodality chelation; MSAP, multifunctional single-attachment point; NHS, *N*-hydroxysuccinimide; NIRF, near-infrared fluorescence; QY, quantum yield; RB, relative brightness; RCY, radiochemical yield; SPPS, solid-phase peptide synthesis; TAC, time−activity-curve; TETA, 1,4,8,11-tetraazacyclotetradecane-*N*,*N*′,*N*″,*N*‴-tetraacetic acid

REFERENCES

(1) Histed, S. N.; Lindenberg, M. L.; Mena, E.; Turkbey, B.; Choyke, P. L.; Kurdziel, K. A. Review of functional/anatomical imaging in oncology. *Nucl. Med. Commun.* **2012**, *33*, 349−361.

(2) Culver, J.; Akers, W.; Achilefu, S. Multimodality molecular imaging with combined optical and SPECT/PET modalities. *J. Nucl. Med.* **2008**, *49*, 169−172.

(3) Sevick-Muraca, E. M. Translation of near-infrared fluorescence imaging technologies: emerging clinical applications. *Annu. Rev. Med.* **2012**, *63*, 217−231.

(4) Gioux, S.; Choi, H. S.; Frangioni, J. V. Image-guided surgery using invisible near-infrared light: fundamentals of clinical translation. *Mol. Imaging* **2010**, *9*, 237−255.

(5) van Dam, G. M.; Themelis, G.; Crane, L. M.; Harlaar, N. J.; Pleijhuis, R. G.; Kelder, W.; Sarantopoulos, A.; de Jong, J. S.; Arts, H. J.; van der Zee, A. G.; Bart, J.; Low, P. S.; Ntziachristos, V. Intraoperative tumor-specific fluorescence imaging in ovarian cancer by folate receptor-α targeting: first in-human results. *Nat. Med.* **2011**, *17*, 1315−1319.

(6) Sevick-Muraca, E. M.; Sharma, R.; Rasmussen, J. C.; Marshall, M. V.; Wendt, J. A.; Pham, H. Q.; Bonefas, E.; Houston, J. P.; Sampath, L.; Adams, K. E.; Blanchard, D. K.; Fisher, R. E.; Chiang, S. B.; Elledge, R.; Mawad, M. E. Imaging of lymph flow in breast cancer patients after microdose administration of a near-infrared fluorophore: feasibility study. *Radiology* **2008**, *246*, 734−741.

(7) Buckle, T.; Chin, P. T.; van Leeuwen, F. W. (Non-targeted) radioactive/fluorescent nanoparticles and their potential in combined pre- and intraoperative imaging during sentinel lymph node resection. *Nanotechnology* **2010**, *21*, 482001.

(8) Azhdarinia, A.; Ghosh, P.; Ghosh, S.; Wilganowski, N.; Sevick-Muraca, E. M. Dual-labeling strategies for nuclear and fluorescence molecular imaging: a review and analysis. *Mol. Imaging Biol.* **2012**, *14*, 261−276.

(9) Kuil, J.; Velders, A. H.; van Leeuwen, F. W. Multimodal tumor-targeting peptides functionalized with both a radio- and a fluorescent label. *Bioconjugate Chem.* **2010**, *21*, 1709−1719.

(10) Sampath, L.; Kwon, S.; Hall, M. A.; Price, R. E.; Sevick-Muraca, E. M. Detection of cancer metastases with a dual-labeled near-infrared/positron emission tomography imaging agent. *Transl. Oncol.* **2010**, *3*, 307−217.

(11) Zhang, Y.; Hong, H.; Engle, J. W.; Yang, Y.; Theuer, C. P.; Barnhart, T. E.; Cai, W. Positron emission tomography and optical imaging of tumor CD105 expression with a dual-labeled monoclonal antibody. *Mol. Pharm.* **2012**, *9*, 645−653.

(12) Hall, M. A.; Kwon, S.; Robinson, H.; Lachance, P. A.; Azhdarinia, A.; Ranganathan, R.; Price, R. E.; Chan, W.; Sevick-Muraca, E. M. Imaging prostate cancer lymph node metastases with a multimodality contrast agent. *Prostate* **2012**, *72*, 129−146.

(13) Garanger, E.; Aikawa, E.; Reynolds, F.; Weissleder, R.; Josephson, L. Simplified syntheses of complex multifunctional nanomaterials. *Chem. Commun. (Cambridge, U. K.)* **2008**, 4792−4794.

(14) Xu, H.; Baidoo, K.; Gunn, A. J.; Boswell, C. A.; Milenic, D. E.; Choyke, P. L.; Brechbiel, M. W. Design, synthesis, and characterization of a dual modality positron emission tomography and fluorescence imaging agent for monoclonal antibody tumor-targeted imaging. *J. Med. Chem.* **2007**, *50*, 4759−4765.

(15) Liu, S.; Li, D.; Huang, C. W.; Yap, L. P.; Park, R.; Shan, H.; Li, Z.; Conti, P. S. Efficient construction of PET/fluorescence probe based on sarcophagine cage: an opportunity to integrate diagnosis with treatment. *Mol. Imaging Biol.* **2012**, *14*, 718−724.

(16) Sherry, A. D.; Caravan, P.; Lenkinski, R. E. Primer on gadolinium chemistry. *J. Magn. Reson. Imaging* **2009**, *30*, 1240−1248.

(17) Gabriel, M.; Oberauer, A.; Dobrozemsky, G.; Decristoforo, C.; Putzer, D.; Kendler, D.; Uprimny, C.; Kovacs, P.; Bale, R.; Virgolini, I. J. ^{68}Ga-DOTA-Tyr3-octreotide PET for assessing response to somatostatin-receptor-mediated radionuclide therapy. *J. Nucl. Med.* **2009**, *50*, 1427−1434.

(18) de Jong, M.; Breeman, W. A.; Valkema, R.; Bernard, B. F.; Krenning, E. P. Combination radionuclide therapy using ^{177}Lu- and ^{90}Y-labeled somatostatin analogs. *J. Nucl. Med.* **2005**, *46* (Suppl. 1), 13S−17S.

(19) Bodei, L.; Cremonesi, M.; Grana, C. M.; Fazio, N.; Iodice, S.; Baio, S. M.; Bartolomei, M.; Lombardo, D.; Ferrari, M. E.; Sansovini, M.; Chinol, M.; Paganelli, G. Peptide receptor radionuclide therapy with (177)Lu-DOTATATE: the IEO phase I-II study. *Eur. J. Nucl. Med. Mol. Imaging* **2011**, *38*, 2125−2135.

(20) Zhernosekov, K. P.; Filosofov, D. V.; Baum, R. P.; Aschoff, P.; Bihl, H.; Razbash, A. A.; Jahn, M.; Jennewein, M.; Rosch, F. Processing of generator-produced ^{68}Ga for medical application. *J. Nucl. Med.* **2007**, *48*, 1741−1748.

(21) Wadas, T. J.; Wong, E. H.; Weisman, G. R.; Anderson, C. J. Copper chelation chemistry and its role in copper radiopharmaceuticals. *Curr. Pharm. Des.* **2007**, *13*, 3−16.

(22) Rossin, R.; Kohno, T.; Hagooly, A.; Sharp, T.; Gliniak, B.; Arroll, T.; Chen, Q.; Hewig, A.; Kaplan-Lefko, P.; Friberg, G.; Radinsky, R.; Evelhoch, J. L.; Welch, M. J.; Hwang, D. R. Characterization of ^{64}Cu-DOTA-conatumumab: a PET tracer for in vivo imaging of death receptor 5. *J. Nucl. Med.* **2011**, *52*, 942−949.

(23) Bryan, J. N.; Jia, F.; Mohsin, H.; Sivaguru, G.; Anderson, C. J.; Miller, W. H.; Henry, C. J.; Lewis, M. R. Monoclonal antibodies for copper-64 PET dosimetry and radioimmunotherapy. *Cancer Biol. Ther.* **2011**, *11*, 1001−1007.

(24) Houston, J. P.; Ke, S.; Wang, W.; Li, C.; Sevick-Muraca, E. M. Quality analysis of in vivo near-infrared fluorescence and conventional γ images acquired using a dual-labeled tumor-targeting probe. *J. Biomed. Opt.* **2005**, *10*, 054010.

(25) Li, C.; Wang, W.; Wu, Q.; Ke, S.; Houston, J.; Sevick-Muraca, E.; Dong, L.; Chow, D.; Charnsangavej, C.; Gelovani, J. G. Dual optical and nuclear imaging in human melanoma xenografts using a single targeted imaging probe. *Nucl. Med. Biol.* **2006**, *33*, 349−358.

(26) Adams, K. E.; Ke, S.; Kwon, S.; Liang, F.; Fan, Z.; Lu, Y.; Hirschi, K.; Mawad, M. E.; Barry, M. A.; Sevick-Muraca, E. M. Comparison of visible and near-infrared wavelength-excitable fluorescent dyes for molecular imaging of cancer. *J. Biomed. Opt.* **2007**, *12*, 024017.
(27) Marshall, M. V.; Draney, D.; Sevick-Muraca, E. M.; Olive, D. M. Single-dose intravenous toxicity study of IRDye 800CW in Sprague-Dawley rats. *Mol. Imaging Biol.* **2010**, *12*, 583−594.
(28) Cai, H.; Li, Z.; Huang, C. W.; Park, R.; Shahinian, A. H.; Conti, P. S. An improved synthesis and biological evaluation of a new cage-like bifunctional chelator, 4-((8-amino-3,6,10,13,16,19-hexaazabicyclo[6.6.6]icosane-1-ylamino)methyl)benzoic acid, for ^{64}Cu radiopharmaceuticals. *Nucl. Med. Biol.* **2010**, *37*, 57−65.
(29) Anderson, C. J.; Ferdani, R. Copper-64 radiopharmaceuticals for PET imaging of cancer: advances in preclinical and clinical research. *Cancer Biother. Radiopharm.* **2009**, *24*, 379−393.
(30) Dumont, R. A.; Deininger, F.; Haubner, R.; Maecke, H. R.; Weber, W. A.; Fani, M. Novel (64)Cu- and (68)Ga-labeled RGD conjugates show improved PET imaging of α(v)β(3) integrin expression and facile radiosynthesis. *J. Nucl. Med.* **2011**, *52*, 1276−1284.
(31) Azhdarinia, A.; Wilganowski, N.; Robinson, H.; Ghosh, P.; Kwon, S.; Lazard, Z. W.; Davis, A. R.; Olmsted-Davis, E.; Sevick-Muraca, E. M. Characterization of chemical, radiochemical and optical properties of a dual-labeled MMP-9 targeting peptide. *Bioorg. Med. Chem.* **2011**, *19*, 3769−3776.
(32) Rodenberg, E.; Azhdarinia, A.; Lazard, Z. W.; Hall, M.; Kwon, S. K.; Wilganowski, N.; Salisbury, E. A.; Merched-Sauvage, M.; Olmsted-Davis, E. A.; Sevick-Muraca, E. M.; Davis, A. R. Matrix metalloproteinase-9 is a diagnostic marker of heterotopic ossification in a murine model. *Tissue Eng., Part A* **2011**, *17*, 2487−2496.
(33) Rogers, B. E.; Anderson, C. J.; Connett, J. M.; Guo, L. W.; Edwards, W. B.; Sherman, E. L.; Zinn, K. R.; Welch, M. J. Comparison of four bifunctional chelates for radiolabeling monoclonal antibodies with copper radioisotopes: biodistribution and metabolism. *Bioconjugate Chem.* **1996**, *7*, 511−522.
(34) Hall, M. A.; Pinkston, K. L.; Wilganowski, N.; Robinson, H.; Ghosh, P.; Azhdarinia, A.; Vazquez-Arreguin, K.; Kolonin, A. M.; Harvey, B. R.; Sevick-Muraca, E. M. Comparison of mAbs targeting epithelial cell adhesion molecule for the detection of prostate cancer lymph node metastases with multimodal contrast agents: quantitative small-animal PET/CT and NIRF. *J. Nucl. Med.* **2012**, *53*, 1427−1437.
(35) Weissleder, R.; Tung, C. H.; Mahmood, U.; Bogdanov, A., Jr. In vivo imaging of tumors with protease-activated near-infrared fluorescent probes. *Nat. Biotechnol.* **1999**, *17*, 375−378.
(36) Sun, M. M.; Beam, K. S.; Cerveny, C. G.; Hamblett, K. J.; Blackmore, R. S.; Torgov, M. Y.; Handley, F. G.; Ihle, N. C.; Senter, P. D.; Alley, S. C. Reduction-alkylation strategies for the modification of specific monoclonal antibody disulfides. *Bioconjugage Chem.* **2005**, *16*, 1282−1290.
(37) Rossin, R.; Verkerk, P. R.; van den Bosch, S. M.; Vulders, R. C.; Verel, I.; Lub, J.; Robillard, M. S. In vivo chemistry for pretargeted tumor imaging in live mice. *Angew. Chem., Int. Ed.* **2010**, *49*, 3375−3378.
(38) Williams, A. T. R.; Winfield, S. A.; J.N., M. Relative fluorescence quantum yields using a computer controlled luminescence spectrometer. *Analyst* **1983**, *108*, 1067−1071.
(39) Sevick-Muraca, E. M.; Heintzelman, D. L.; Lee, J.; Troy, T. L.; Paithankar, D. Y. Role of higher-order scattering in solutions to the forward and inverse optical-imaging problems in random media. *Appl. Opt.* **1997**, *36*, 9058−9067.
(40) Poczatek, R. B.; Myers, R. B.; Manne, U.; Oelschlager, D. K.; Weiss, H. L.; Bostwick, D. G.; Grizzle, W. E. Ep-Cam levels in prostatic adenocarcinoma and prostatic intraepithelial neoplasia. *J. Urol.* **1999**, *162*, 1462−1466.
(41) Hall, M. A.; Aldrich, M. B.; Azhdarinia, A.; Lachance, P. A.; Robinson, H.; Hazen, A.; Haviland, D. L.; Sevick-Muraca, E. M. Quantifying multimodal contrast agent biological activity using near-infrared flow cytometry. *Contrast Media Mol. Imaging* **2012**, *7*, 338−345.